Quality mapping of aluminium alloy diecastings

Giulio Timelli, Franco Bonollo
Department of Management and Engineering, University of Padova, Vicenza, Italy

ABSTRACT

The effect of casting defects on mechanical properties was investigated for a high-pressure die-cast aluminium alloy. A series of U-shaped components were cast using a fully controlled cold chamber high-pressure die-casting machine with different process parameters. Defects existed in gas and shrinkage pores as well as oxide inclusions. An X-ray equipment was used for a preliminary quality control but showed its limits in detecting defects. The castings were sectioned and tensile bars extracted from different locations in the castings in order to map the distribution of the mechanical properties. The decrease in mechanical properties correlated with the area fractions of defects revealed on the fracture surface of the tensile specimens. A quality mapping approach showed how the final properties depend on the position of the casting and the process parameters adopted.

RIASSUNTO

Nel presente lavoro si è studiata l'influenza dei difetti sulle caratteristiche meccaniche di getti pressocolati in lega d'alluminio. È stata colata una serie di componenti con profilo ad U utilizzando una tecnologia di pressocolata in camera fredda e una variazione sistematica dei parametri di processo. I difetti più comuni riscontrati sono state cavità da ritiro o porosità dovute a intrappolamento di gas, ed inclusioni di ossidi. Per le analisi preliminari di tipo qualitativo sui componenti colati, è stato utilizzato un impianto radioscopico che ha però rivelato i propri limiti nell'individuazione dei difetti presenti. Diverse zone del getto hanno fornito campioni per prove statiche a trazione; lo studio di questi ha permesso di redigere una mappatura della distribuzione delle caratteristiche meccaniche all'interno del getto stesso. La diminuzione delle proprietà meccaniche è proporzionale all'area occupata dai difetti sulla superficie di frattura dei campioni di trazione. La valutazione della qualità dei getti pressocolati in lega d'alluminio ha permesso di evidenziare come le proprietà meccaniche finali si distribuiscano sulla base dei parametri di processo utilizzati.

KEYWORDS

High-pressure die-casting; Aluminium alloy; Defects; Oxide inclusions; Porosity; Fractography; X-ray radiography; Mechanical properties.

INTRODUCTION

High-pressure die-casting (HPDC) is widely used for the possibility of obtaining net to shape components of complex geometry and thin wall thickness at high production rates [1,2]. However, a number of parameters exists, which, if not adequately determined and adjusted, result in a decadence of quality of the die cast part. Common defects in manufactured parts are shrinkage cavities, cold fills, oxide films, dross, entrapped air bubbles. One of the major source of defects in HPDC is air entrapment in the melt during the filling stage of the die, but a detrimental effect can also come from defects generated in the shot sleeve before and during the injection process [3,4]. The influence of casting defects on the mechanical properties of cast aluminium alloys has been investigated by a number of researchers, with the common conclusion that defects can make the tensile behaviour of casting alloys unpredictable. Castings with thin sections, like those produced by HPDC technology, are vulnerable to the effect of defects since a single macrodefect can cover a significant fraction of the cross-section area. Even high integrity castings are expected to contain defects and thus it is important to predict their effect on final mechanical properties of the material. Campbell [5] and Dai et al. [6,7] showed that improper design of the filling system results in higher turbulence so that oxide films are generated and entrapped into the bulk liquid metal. Ingate velocities significantly affect the number and distribution of the oxide film defects generated from filling stage. Cáceres et al. [8] and Gokhale et al. [9] demonstrated how the mechanical properties decrease monotonically with an increase in the area fraction of defects revealed on the fracture surface of gravity cast aluminium specimens. Avalle et al. [2] and Wang et al. [10,11] studied the effect of defects on fatigue behaviour of cast aluminium alloys showing how casting defects have a detrimental effect by shortening not only fatigue crack propagation, but also initiation period, which is influenced by defects' size. They also showed how castings with defects have at least an order of magnitude lower fatigue life compared to defect-free materials and how porosity is more detrimental to fatigue life than oxide films. In literature data, static strength appears to be modestly influenced by casting defects compared to the elongation to fracture [2,3,8,9].

Generally, the effect of porosity on

mechanical properties is studied through the measurement of the defect volume fractions or X-ray analysis, but these methods have the disadvantage to not reveal the presence of detrimental oxide films [12]. Therefore, quantitative fractography became a useful tool for such study because the fracture surface of tensile bars contains the part of the microstructure and defects that affect and govern the fracture mechanism. If the fracture surface is large enough, there is a likely to be a discernible pattern of chevron marks that leads to the point at which fracture was initiated [13]. Examination of this initiation point or region can reveal if fracture was initiated from a structural defect or a microstructural feature. Non-destructive methods are also adopted, such as acoustic microscope, which are able to detect cold flakes, especially the oxide layers, better than X-ray radiography [12,14]. A better correlation and reduced scatter is then obtained if the decrease in tensile strength and elongation to fracture are plotted against the projected area of defects on the fracture surface, instead of defect volume fractions.

Almost all the above mentioned researches were based on gravity cast testing specimens separately poured in sand/chill mold, where the amount of defects was generated avoiding degassing, vigorously stirring the melt, or controlling the feeding and pouring temperature. On industrial HPDC production it is more difficult to control the amount and type of defects due to the complexity of the casting shape or to variable parameters such as the mold temperature, dosing volume, slow and fast shots, commutation points, injection and upset pressure. Therefore, a quality mapping approach could be the right path to lead to the quantitative extended prediction of HPDC properties.

In this work a HPDC component was analysed and a combination of injection parameters and pouring temperatures were adopted in order to generate different type and amount of casting defects. The material was an EN AC-46000 aluminium alloy, widely used in load bearing components in automotive field. X-ray inspection was preliminary carried out in different zones of the casting and in tensile bars extracted from the components, while fractography analysis was carried out to detect the projected area of defects on fracture surface to quantify their effect on the mechanical behaviour.

EXPERIMENTAL PROCEDURE

CASTING EXPERIMENT

For R&D purposes, a die for casting U-shaped of aluminium alloys has been made. The CAD model of aluminium casting with runners, gating and overflow system is displayed in figure 1a. The U-shaped casting was coupled with ribs, which are generally a location with high defect concentration. Figure 1b shows an example of an interrupted filling of the die with the arrow indicating a location where two metal flows meet. The die-castings, with wall thickness ranging from 2.5 mm through 6 mm, were produced in a Müller-Weingarten 750 ton cold chamber die-casting machine, with a shot chamber length of 580 mm and diameter of 70 mm. The fill fraction of the shot sleeve was kept constant at 0.56 and every shot was documented with its shot profile. Temperature measurements were performed regularly, both using an infrared camera and temperature probes and the furnace temperature was checked frequently. Manual spraying and blowing process were used in order to cool down
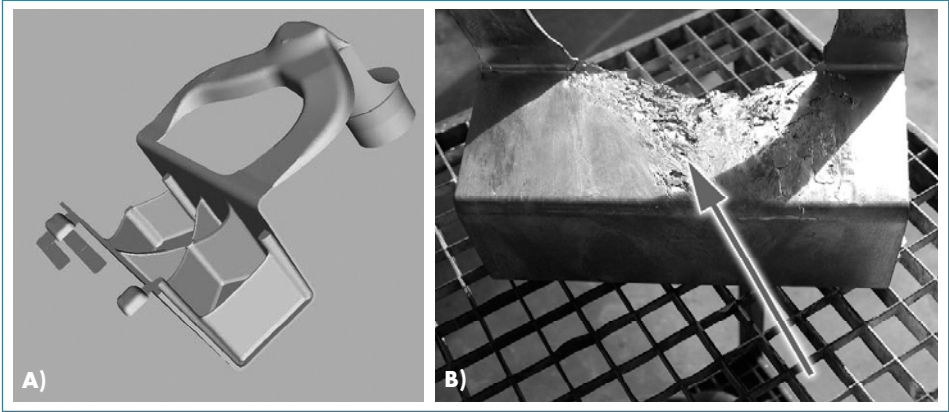

Fig. 1: a) The U-shaped CAD geometry (Length: 260 mm, height: 110 mm, width: 70 mm, outer wall thickness: 2.5 mm, rib thickness: 4-6 mm); b) Interrupted filling of the die. The arrow indicates a location where two metal flows meet.

properly the die material and aid the release of the casting after complete solidification. After-pressure was also adopted to ensure the proper ejection of the parts.

In the present work an EN AC-46000 aluminium alloy (European designation, equivalent to the US designation A380), according UNI EN 1706, with composition listened in table 1, was cast. This alloy has a liquidus-solidus temperature range of approximately 593-538°C [15].

The U-shaped castings were produced with the process parameters indicated in table 2. The shot profiles can also be seen in figure 2. Throughout this paper, the different process parameters will be termed P1,..., P4 and T2 respectively.

Table 1. Chemical composition of the casting alloy (wt.%)

Alloy	Si	Mg	Cu	Fe	Mn	Zn	Ni	Cr	Ti	Al.
EN AC-46000	9.87	0.22	2.441	0.758	0.216	0.467	0.059	0.018	0.07	bal.

In the profile P1, the plunger speed was kept constant in the first phase and a rapid acceleration was applied in the second phase, i.e. at the beginning of die filling. The same profile was adopted for T2 but the pouring temperature was 50°C lower. For the other shot profiles the plunger was accelerated slowly also in the first phase, trying however to minimize air entrapment in the slow shot. The main differences regarded the variations of the switch point

Shot profile	Plunger velocity slow shot (ms^{-1})	Plunger velocity fast shot (ms^{-1})	Commutation point slow-fast shot (mm)	Commutation point to upset pressure (mm)	Ingate velocity (ms^{-1})	Pouring temperature (°C)
P1	0.4	3	428	552	48.9	690
P2	0.4-0.6	3	447	562	48.9	690
P3	0.4-0.7	2	373	544	32.9	690
P4	0.4-0.6	2	451	547	32.9	690
T2	0.4	3	428	552	48.9	640
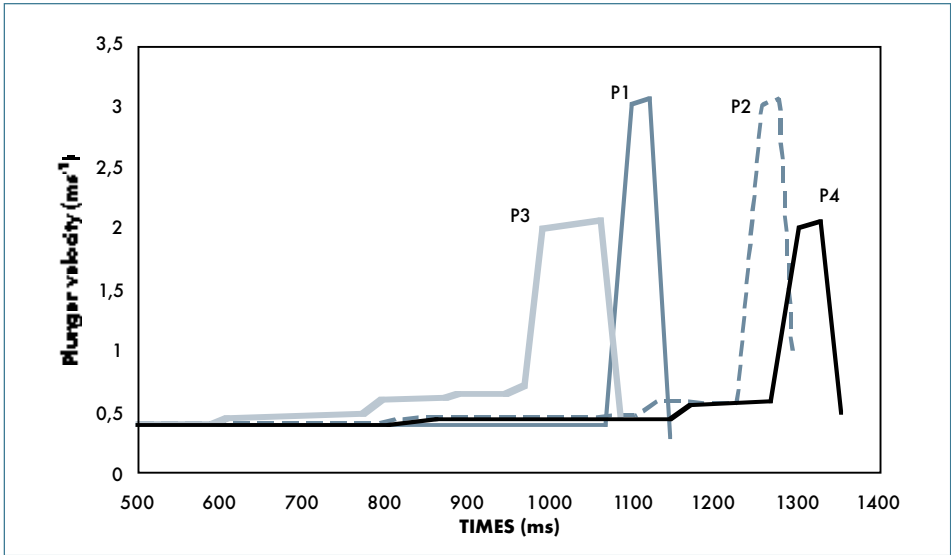
Fig. 2: Different shot profiles used in the present work.

Fig. 3: Thermal management of the die.

between the first and second phase, where the commutation point was anticipated (P3) and postponed (P2 and P4), and the reduction of the plunger velocity in the second phase for the profiles P3 and P4.

The shot sleeve and the die were preheated but reached a quasi-steady state temperature after some shots, thus the first several castings were scrapped. Figure 3 shows the cooling system adopted to stabilise the temperature of the die and of the shot sleeve.

X-RAY, TENSILE TESTS AND MICROSTRUCTURAL INVESTIGATIONS

The U-shaped die-castings were mapped throughout with a macro-focus X-ray equipment for a preliminary analysis and comparison.

Tensile test bars with a rectangular cross section were extracted from eight different locations of the castings and the gauge length examined, pre and after the tensile testing, with a micro-focus X-ray equipment, which can magnify an image several times while still offering a better definition than a conventional X-ray tube. Throughout this paper, the different locations will be termed zones 1,...,8 respectively. The locations and the main dimensions of the tensile specimens are indicated in figure 4 and table 3. The X-ray images were then analysed using a commercial image-analysis software package. The defect area of each image was evaluated by counting the image pixels in each defect (figure 5). Every defect was counted indifferently.
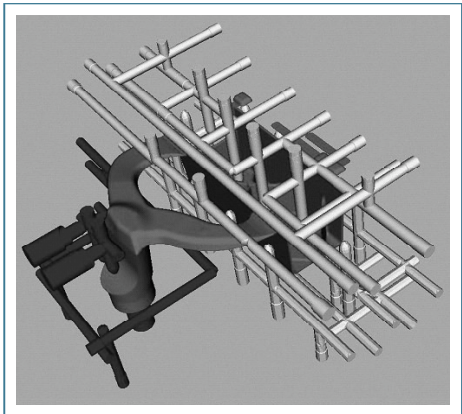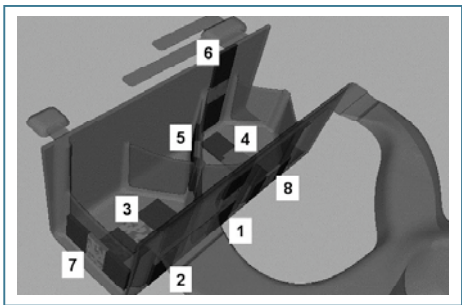

Fig. 4: U-shaped die casting with investigated locations.

	zone 1,2 (mm)	zone 3,4,7 (mm)	zone 5 (mm)	zone 6 (mm)	zone 8 (mm)
Gauge length	60	30	26	60	30
Thickness	2.5	3.1	6	4.1	2.4
Width	10	10	10	10	10

The tensile strength, UTS (MPa), and the engineering elongation to fracture, s_f, of each sample were converted to true tensile strength (σ_f) and true elongation to fracture (ε_f) through equations [16, 17]:

$$\sigma_f = UTS(1 + s_f) \qquad (1)$$

$$\varepsilon_f = 1n(1 + s_f) \qquad (2)$$

The true stress (σ)-true plastic strain (ε) flow curves of each specimen were approximated with a constitutive equation of the form [16, 17]:

$$\sigma = K\varepsilon^n \qquad (3)$$

where K is the alloy's strength coefficient and n the strain hardening exponent. The Quality Index, Q (MPa), defined [16-18] as

$$Q = UTS + 0.4K\log(100 \cdot s_f) \qquad (4)$$
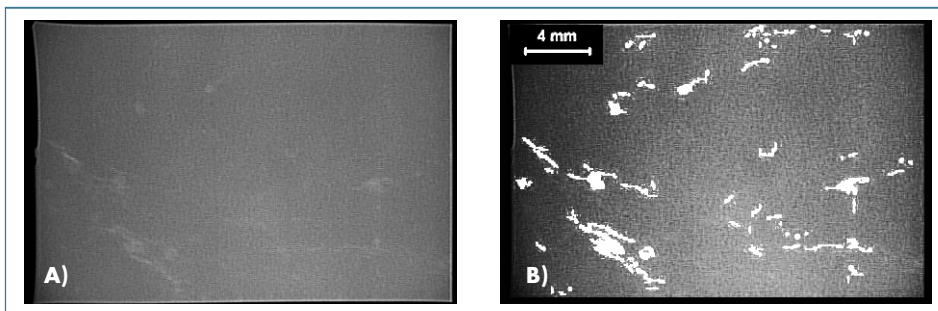
was then considered.

Fig. 5: (a) X-ray image; (b) the same X-ray image binarized to determine the amount of defects.

The fractured surfaces after testing were then observed under an optical stereomicroscope at a magnification of about x10. The acquired images were then transferred into a single photograph and the area of defects was measured by using an image analyser. The total measured defect area was then divided by the initial cross section of the sample to find the defect area fraction. A scanning electron microscope was also used as support for the fractographic analysis.

At least three different castings from every shot profile were chosen to be analysed according to the described procedure.

RESULTS AND DISCUSSION

X-RAY ANALYSIS

The X-ray images in figure 6 are taken from zone 2 of three consecutive U-shaped castings poured according the profile P4. The size and the distribution of defects is different in spite the same process parameters were adopted. It is evident how the formation of defects is sensitive to small variations in the casting conditions and the causes cannot be only connected to the process profile adopted, even if this variable results the main source of defects. Figure 7 shows the X-ray pictures, taken with macro- and micro-focus, from a tensile bar extracted from zone 2 of a casting poured according to the profile P4. The micro-focus pictures show defects and details not appreciable with conventional X-ray tube. The defects seem to result from local die filling condition, i.e. a vortex, as indicated by arrows, was generated in the zone 2, entrapping and dragging air bubbles.

The results of the X-ray image analysis of zones 1 and 2 are shown in figures 8 and 9. While figure 8 shows the defect distribution in zones 1 and 2 of castings poured with different shot profiles, evidencing the influence of process
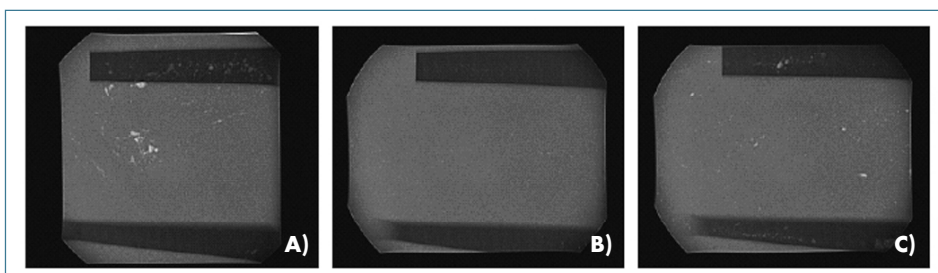

Fig. 6: Macro-focus X-ray images taken from zone 2 of three different castings consecutively poured with shot profile P4.
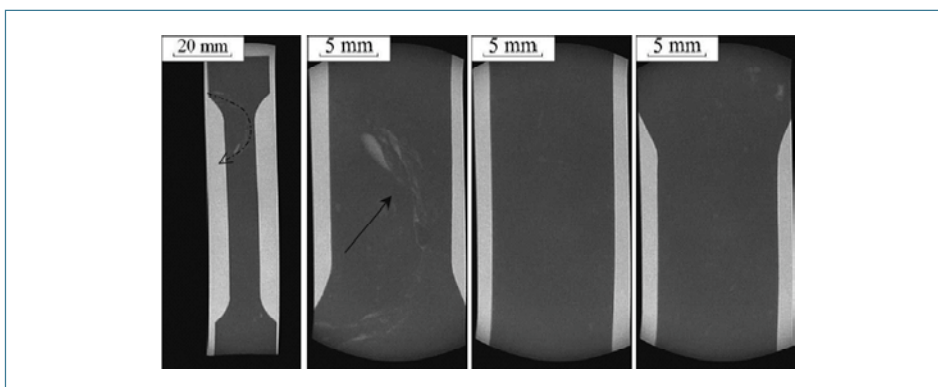

Fig. 7: Macro- and micro-focus X-ray images taken in a tensile bar extracted from zone 2 of a casting poured with shot profile P4.

parameters in the amount of defects, figure 9 demonstrates how, in three consecutive castings poured with the process P4, the defect reproducibility is sensitive to small uncontrolled variations of the casting conditions, and how the amount of defects cannot be controlled only by changing shot profiles.

The same X-ray analysis was then repeated in the fractured tensile bars to characterize the position of the fracture into the whole bar. The analysis underlined how the fracture developed in the presence of defects (figure 10), but sometime the fracture path took place in a zone where the X-ray radiography didn't show any defect (figure 11). In these cases, the following fractographic inspection revealed a high amount of oxide inclusions, which represent surfaces of discontinuity in the material and point for crack initiation. The oxide films were not revealed by X-ray inspection because the difference of density between the aluminium alloy and the aluminium oxide skins is minimum and thus not detectable through conventional X-ray technique [12].

MECHANICAL PROPERTIES

From the tensile test results, it was possible to observe how the amount of defects influenced considerably the UTS and the elongation to fracture (s_f), which ranged from 129 to 307 MPa and from 0.29% to 2.89% respectively. If elastic properties of the material, as the Young modulus (E) and the Yield Strength ($YS_{0.2\%}$), were
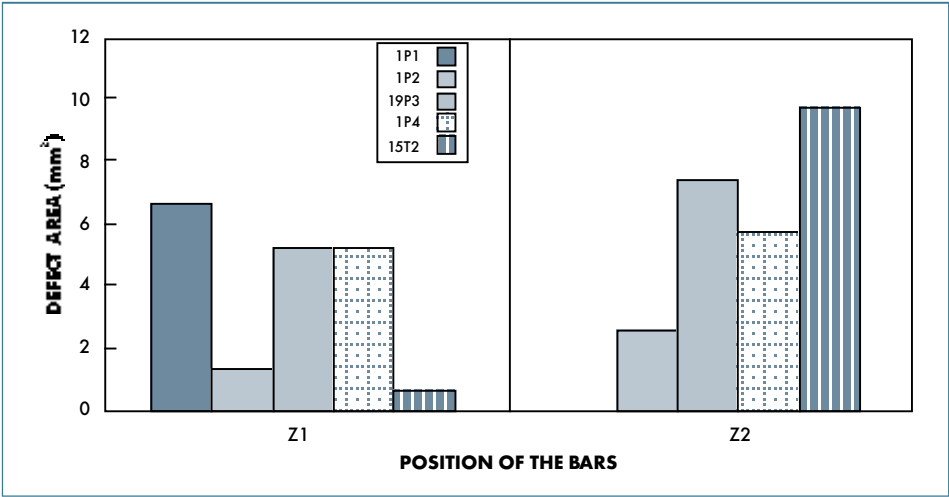
Fig. 8: Distribution of defects in zones 1 (Z1) and 2 (Z2) of castings poured with different process parameters.
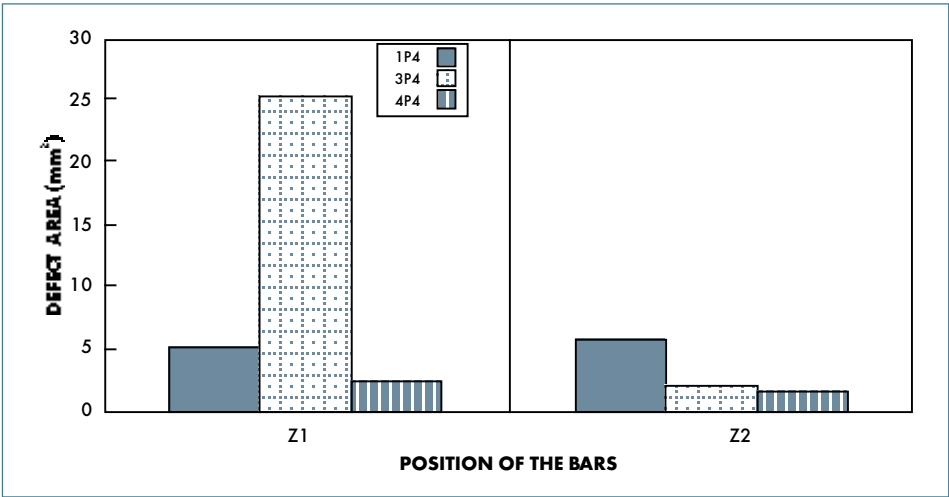
Fig. 9: Distribution of defects in zones 1 (Z1) and 2 (Z2) of three different castings consecutively poured with shot profile P4.
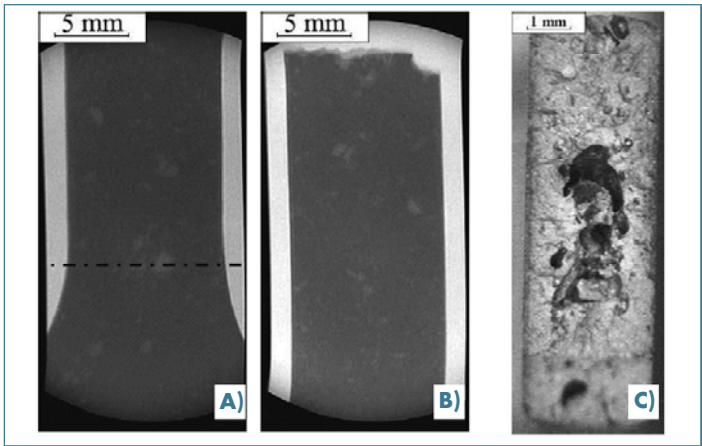
Fig. 10: X-ray images of a tensile bar (a) before and (b) after testing; (c) fracture surface. The line in (a) represents the fracture path in the specimen. Defects were detectable by X-ray inspection.
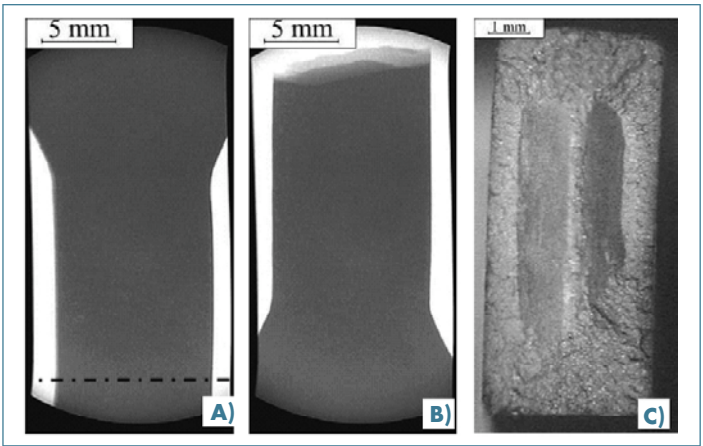
Fig. 11: X-ray images of a tensile bar (a) before and (b) after testing; (c) fracture surface. The line in (a) represents the fracture path in the specimen. Defects were not detectable by X-ray inspection.

considered, all data arranged around constant values, (72 GPa and 180 MPa respectively) independently from the zone of extraction, the process parameters, but above all the amount of defects. Plotting the true stress-true plastic strain flow curves of each specimen and the mean flow curve (figure 12), according eq. (3), it is possible to observe how all the curves followed a similar trend and the difference consisted in the break point, i.e. the fracture. Considering the same graph with the mean flow curve but plotting the true tensile strength (σ_f) and the true elongation to fracture (ε_f) values obtained according eqs. (1) and (2), a better view of what previously said is shown (figure 13). The scattering of data from the mean flow curve

$$\sigma = 755\varepsilon^{0.23} \qquad (5)$$

is low, as shown by the coefficient of determination, R^2, equal to 0.95.

Therefore, eq. (5) can be considered constitutive of the uniform plastic behaviour of the alloy analysed. To understand the correlation between the fracture and the amount of defects, the bubble plot in figure 14 can be considered where each bubble represents the true tensile strength (σ_f) and the true elongation to fracture (ε_f) and the diameter of the bubble is proportional to the defect area fraction. Increasing the distance from the origin, the diameter of the bubbles and therefore the defect area fraction decreases, indicating the fundamental role of defects on fracture mechanism. A similar graph can be seen in figure 15 where the diameter of each bubble is instead proportional to the Quality Index, defined by eq. (4). Quality
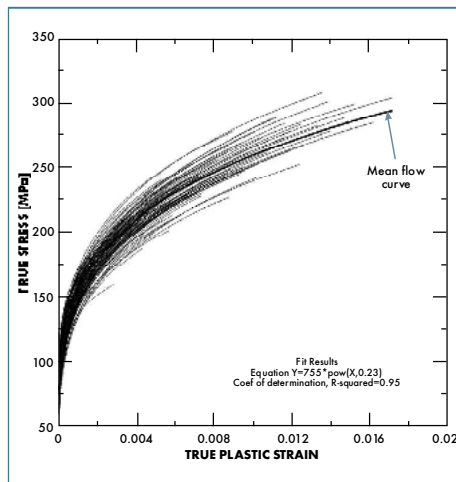

Fig. 12: The true stress-true plastic strain flow curves of each specimen and the mean flow curve, according eq. (3).
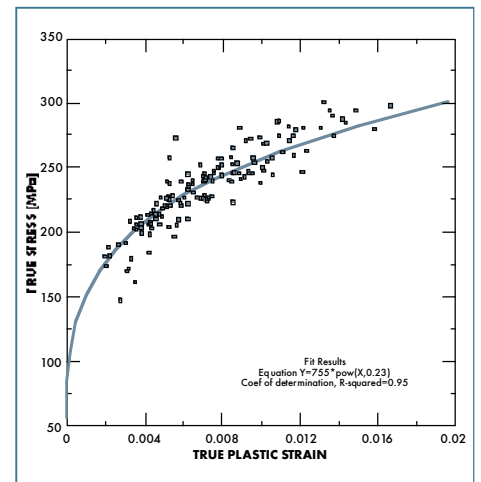

Fig. 13: The true tensile strength (σ_f) and true elongation to fracture (ε_f) values of each sample obtained according eqs. (1) and (2) are plotted together with the mean flow curve.
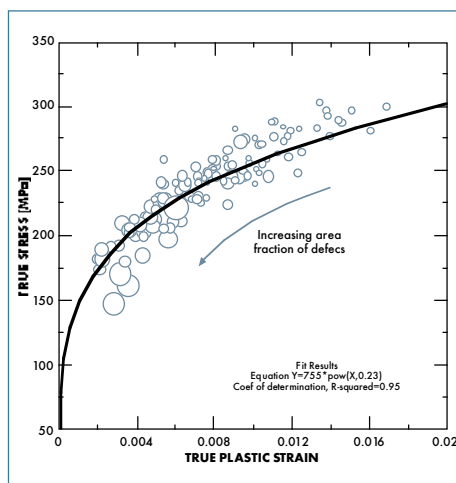

Fig. 14: Bubble plot of the true tensile strength (σ_f) and true elongation to fracture (ε_f) values of each sample where the diameter of each bubble is proportional to the defect area fraction.
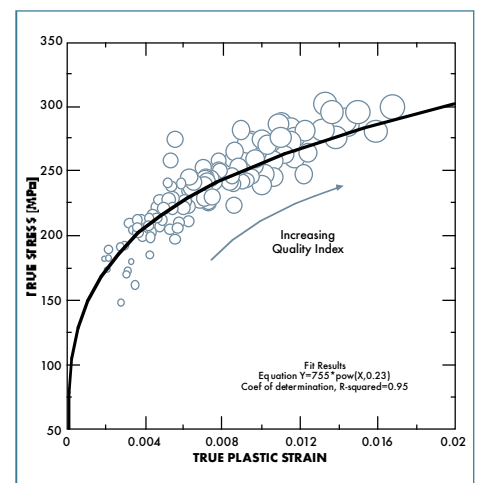

Fig. 15: Bubble plot of the true tensile strength (σ_f) and true elongation to fracture (ε_f) values of each sample where the diameter of each bubble is proportional to the Quality Index.
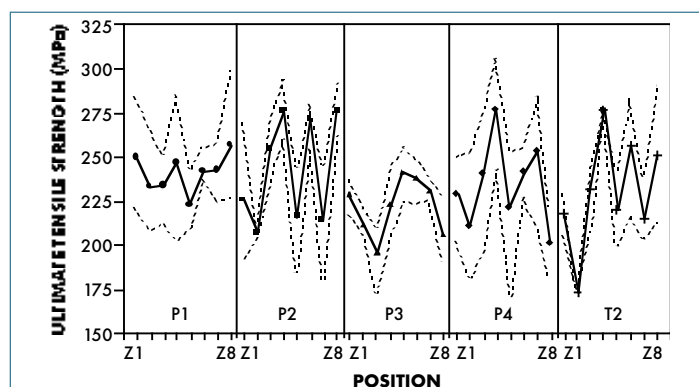

Fig. 16. The mean UTS, together with the scattering bands, is plotted versus the different positions (Z1,...,Z8) and process parameters adopted.
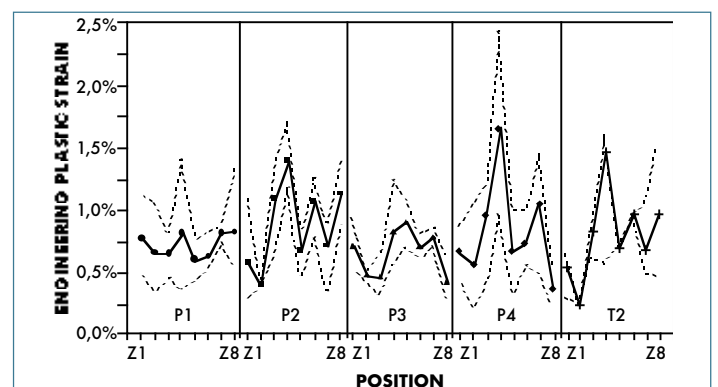

Fig. 17: The mean engineering plastic strain, together with the scattering bands, is plotted versus the different positions (Z1,...,Z8) and process parameters adopted.

Index has the advantage to consider both tensile and strain properties of the material at the same time. As expected, the general trend of the graph is opposite to the previous one, showing thus the strict relationship with the defect amount.

The final quality maps can be seen in figures 16 and 17 where the mean mechanical properties, together with the scattering bands (minimum and maximum values), are plotted versus the different positions (Z1,...,Z8) and process parameters adopted. In general, it can be seen how, considering the same position, the UTS and the engineering plastic strain show different values changing the process parameters; while, fixing the process variables, the mechanical properties change with changing location. Therefore, from these considerations it is possible to understand the difficulty in optimising the whole casting and the HPDC process parameters.

CONCLUSIONS

The primary objective of this work has been to characterize the influence of casting defects on mechanical properties of a high-pressure aluminium U-shaped casting. From the experimental findings it can be concluded that:

1. The amount and type of defects changes by changing the process parameters.

2. The size and distribution of defects are different inside the casting in spite the same process parameters are adopted.

3. An X-ray technique reveals its limit in detecting the presence of oxide inclusions.

4. The amount of defects influences considerably the plastic properties of the material but not the elastic characteristics.

5. A constitutive equation, $\sigma = K\varepsilon^n$, can be considered as representative of the uniform plastic behaviour of the alloy, independently of the presence of defects.

6. The defect area fraction, detected on the fracture surface of tensile test specimens, can be used to establish the fracture point along the constitutive equation.

7. A quality mapping approach can be used in high-pressure die-casting to demonstrate how the amount and type of defects, and the mechanical properties are distributed in a casting by changing the process parameters.

ACKNOWLEDGMENTS

REFERENCES

[1] G.O. VERRAN, R.P.K. MENDES and M.A. ROSSI, J. Mater. Process. Technol., (2006), article in press.

[2] M. AVALLE, G. BELINGARDI, M.P. CAVATORTA and R. DOGLIONE, Int. J. Fatigue 24, (2002), pp. 1-9.

[3] F. FAURA, J. LÓPEZ and J.HERNÁNDEZ, Int. J. Mach. Tools Manuf. 41, (2001), pp. 173-191.

[4] H.I. LAUKLI, PhD thesis, Norwegian University Of Science and Technology (NTNU) (Trondheim), 2004.

[5] J. CAMPBELL, Casting. Elsevier Science Ltd., Oxford (2003).

[6] X. DAI, X. YANG, J. CAMPBELL and J. WOOD, Mater. Sci. Eng. A354, (2003), pp. 315-325.

[7] X. DAI, X. YANG, J. CAMPBELL and J. WOOD, Mater. Sci. Technol. 20, (2004), pp. 505-513.

[8] C.H. CÁCERES and B.I. SELLING, Mater. Sci. Eng. A220, (1996), pp. 109-116.

[9] A.M. GOKHALE and G.R. PATEL, Scripta Mater. 52, (2005), pp.237-241.

[10] Q.G. WANG, D. APELIAN and D.A. LADOS, J. Light Met. 1, (2001), pp. 73-84.

[11] Q.G. WANG, D. APELIAN and D.A. LADOS, J. Light Met. 1, (2001), pp. 85-97.

[12] S. FOX and J. CAMPBELL, Scripta Mater. 43, (2000), pp. 881-886.

[13] J.A. FRANCIS and G.M.D. CANTIN, Mater. Sci. Eng. A407, (2005), pp. 322-329.

[14] A.K.M. AZIZ AHAMED, H. KATO, K. KAGEYAMA and T. KOMAZAKI, Mater. Sci. Eng., (2006), article in press.

[15] American Society of Metals (ASM), Casting-Nonferrous casting alloys. ASM Handbook, vol.15, ASM International, Materials Park OH, (1991).

[16] C.H. CÁCERES, Int. J. Cast Metals Res. 12, (2000), pp. 367-375.

[17] C.H. CÁCERES, Int. J. Cast Metals Res. 12, (2000), pp. 385-391.

[18] M. DROUZY, S. JACOB, M. RICHARD, AFS Int. Cast Metals J. 5, (1980), pp. 43-50.